Simulation of the temporal behavior of soliton propagation in photorefractive media

J. Maufoy,[1] N. Fressengeas,[1] D. Wolfersberger,[1,2] and G. Kugel[2]

[1]*Supélec, 2 rue Edward Belin, 57078 Metz Cedex 3, France*

[2]*Laboratoire Matériaux Optiques à Propriétés Spécifiques–CLOES, Université de Metz–Supélec, 2 rue Edouard Belin,*
57078 Metz Cedex 3, France

We consider the propagation of light beams in photorefractive media in the framework of a (1+1)-dimensional model. The Kukhtarev band transport model is introduced both in a time-dependent differential equation describing the evolution of the space charge field and in a nonlinear wave propagation equation. This latter is then numerically solved with a beam propagation method routine. The evolution in time and space of an initially diffracting laser beam is simulated as a function of initial profiles and waists. The beam is shown to go through a transient overfocused state prior to relaxing to a steady state soliton. Additional features such as the stability condition of the system or effects such as optical branching and soliton interactions are studied. [S1063-651X(99)15305-4]

PACS number(s): 42.65.Tg, 42.65.Sf, 42.65.Hw, 42.65.Jx

I. INTRODUCTION

The study of light propagation as spatial soliton beams in photorefractive media is a research topic that began in the early 1990's. It is now widely studied in the general frame of photorefractive nonlinear optics. Since the prevision in 1992 [1,2] of photorefractive spatial solitons and their first experimental observation in 1993 [3,4], this field of both theoretical and experimental investigations had led to the discovery of different types of solitons (quasisteady-state, screening, and photovoltaic soliton) [5–7]. It also allowed a study of new possibilities more recently of applications such as inducting waveguides [8] by solitons or interactions between solitons [9,10].

In 1996, we proposed a theoretical and numerical analysis, based on a (1+1)-dimensional theory, which allowed us to explain the formation of solitons by showing the link existing between the quasi-steady-state soliton and the screening one [11]. This study, using the photorefractive band transport model developed by Kukhtarev *et al.* [12] led to an analytical expression of the space charge field as a function of time allowing the introduction of particular initial conditions. The introduction of this space charge field equation in the wave equation yielded a time-dependent nonlinear wave propagation equation, which governs the conditions of propagation of the light beam in the photorefractive medium.

In order to perform a numerical resolution of this wave equation, we conducted, in previously published papers [11,13], a mathematical treatment based on finding the soliton solution of this equation. This allowed us to deduce the time evolution of the soliton profile, as well as the dependence of its half width at half maximum (HWHM) as a function of one basic parameter which is the ratio r between the peak irradiance and the sum of the background irradiance and the equivalent dark irradiance. This approach, which was, as we will discuss later, highly questionable from the physical point of view, nevertheless led to existence curves of both the quasi-steady-state and screening solitons as a function of the ratio r, comparable to equivalent curves obtained by other authors [14] using alternative and more suitable methods. The assumption that the wave equation, and more precisely, that the light induced refraction index profile supports soliton solutions in both space and time is, in a certain sense, physically incorrect and has to be *a posteriori* ascertained by a systematic resolution of that wave equation. Owing to the complexity of this equation, an analytical resolution is impossible even in the (1+1)-dimensional approximation. Therefore, we propose in the present paper a numerical resolution of the wave equation based on a beam propagation method (BPM) simulation [15]. The photorefractive crystal is supposed to be illuminated with light waves, whose profiles and waists have been obtained using the mathematical approach described in Refs. [11] and [13]. The propagation is then calculated using the split-step Fourier (or BPM) procedure along the propagation axis and as a function of time, the propagation medium being considered as infinitely long and broad. Several effects such as soliton propagation and interactions as well as optical branching [16] are studied using this procedure.

II. THEORETICAL BASIS AND METHOD OF CALCULATION

A. Space charge field and nonlinear wave propagation equation

In the framework of the (1+1)-dimensional [(1+1)D] model [11,13], the space charge field has been shown to follow in time the following time-dependent expression:

$$E_\tau = (E_0 + E_{ph})\exp(-\tau)$$
$$+ [1 - \exp(-\tau)]\left[(E_{ext} + E_{ph})\frac{I_d}{I} - \frac{k_B T}{e}\frac{I'}{I}\right], \quad (1)$$

where E_0 is the initial space charge field, τ is the reduced time to the dielectric relaxation time in the dark, E_{ext} is the applied external electric field, E_{ph} is the photovoltaic equivalent field, and I_d is the artificial dark irradiance. I is the general light intensity (which is the sum of the beam intensity and the dark irradiance), I' its derivative to the trans-

verse variable x; k_B is the Boltzmann constant, T is the temperature, and e is the electron charge.

This space charge field induces, via the electro-optic Pockels effect, a dependence on time of the refractive index profile. This in turn implies that the deduced nonlinear wave equation is also time dependent [11]:

$$\frac{\partial U}{\partial Z} = \frac{i}{2} \frac{\partial^2 U}{\partial X^2} + \{1 - \exp[-(1+|U|^2)\tau]\}$$

$$\times \left(N^2 - D \frac{\partial |U|^2}{\partial X} \right) \frac{U}{1+|U|^2}$$

$$+ E_N(X,Z) \exp[-(1+|U|^2)\tau] U, \qquad (2)$$

where U is the light field normalized to $\sqrt{I_d}$. X and Z are transverse and longitudinal normalized coordinates with

$$X = \frac{x}{X_0}, \quad Z = \frac{z}{kX_0^2}, \qquad (3)$$

where k is the light wave vector. X_0 is a length which can be chosen arbitrarily. (Its value is only a scale factor: changing it does not affect the physical meaning of the result. Let $Z_0 = kX_0^2$ be the normalization factor on the propagation axis.)

$$E_N(X,Z) = E_{\tau(t=0)} \frac{k^2 n^2 r_{\mathrm{eff}} X_0^2}{2}$$

is the normalized generalized initial space charge field. The value of $E_N(X,Z)$ values depends of course on the crystal parameters and history. N is a quantity which is characteristic of the quasi local mechanisms given by the following expression:

$$N^2 = \frac{k^2 n^2 r_{\mathrm{eff}} X_0^2 (E_{\mathrm{ext}} + E_{\mathrm{ph}})}{2}, \qquad (4)$$

where n is the initial index of refraction and r_{eff} is the effective linear electro-optic coefficient. D is a quantity characteristic of the diffusion mechanism of transport and is given by

$$D = \frac{k^2 n^2 r_{\mathrm{eff}} X_0 k_B T}{2e} \qquad (5)$$

B. Soliton profile

In the general case when soliton propagation is considered, the diffusion mechanism is usually neglected, which means in our case that $D = 0$. This is reasonable if, for instance, an external field can be applied, allowing us to overcome the diffusion one. Considering the initial space charge field as uniform $[E_N(X,Z) = N^2]$, a soliton solution of the wave equation (i.e., a solution whose profile does not change throughout the propagation along Z) can be expressed by

$$U(X,Z,\tau) = \sqrt{r} \gamma(X,\tau) \exp(ivZ) \qquad (6)$$

with $\gamma(0,\tau) = 1$ and $\gamma(\pm\infty, \tau) = 0$.

Both experimental and alternative theoretical approaches have proved the existence of these soliton solutions for certain physical conditions in terms of soliton width, trapping field, and r ratio [14]. Their profile $\gamma(X,\tau)$ has to respect the following differential equations:

$$-2v\gamma + \frac{\partial^2 \gamma}{\partial X^2} - \{1 - \exp[-(1+r\gamma^2)\tau]\}$$

$$\times \left(2N^2 \frac{\gamma}{1+r\gamma^2} \right) - 2\gamma \exp[-(1+r\gamma^2)\tau] = 0, \qquad (7)$$

$$v = -\frac{N^2}{r} \ln(1+r) + \frac{N^2}{r} \{Ei[-(1+r)\tau] - Ei(-\tau)\}$$

$$+ \frac{1}{\tau r} \{\exp[-(1+r)\tau] - \exp(-\tau)\}, \qquad (8)$$

where

$$Ei(\tau) = \int_{-\tau}^{+\infty} \frac{e^{-\theta}}{\theta} d\theta.$$

These two differential equations, which in fact define the soliton existence curves, have been numerically used in order to obtain the initial profiles $U(X,00)$ which are introduced at the entrance of the crystal.

Method of calculation

The numerical method used, called in the literature the split-step Fourier method [15], is a beam propagation method (BPM) which has been adapted to solve the nonlinear wave equation (2). As an initial profile at $Z = 0$, we chose functions defined numerically which satisfy Eqs. (7) and (8). The validity of the BPM resolution has been systematically checked by insuring variation of the calculation conditions and parameters. In the simulation undertaken here, we have tested the following behaviors. (a) The space and time convergence towards a screening soliton, (b) the occurrence of a quasi-steady-state soliton, eventually changing to a less focalized beam state, (c) the influence of the drift transport mechanism together with the diffusion one, and (d) the occurrence of optical branching, when high nonlinearities are present.

III. NUMERICAL SIMULATIONS OF SOLITONS TIME BEHAVIOR

In this section, we present results of simulation obtained by the BPM procedure. The data obtained are reported using systematically four or more relevant images chosen from a time-dependent movie at specifically interesting and significant times. The first image always corresponds to the initial time $\tau = 0$ and, thus, to the natural diffraction of the entrance beam with no photorefractive effect, the crystal being considered linear. The last image corresponds to $\tau = 1$, which, in fact appears to be quite similar to the stationary state $\tau = \infty$. The beam propagates from the left to the right along the Z direction. The transverse direction X corresponds to diffraction or focusing direction. The lengths along X and Z are

expressed in normalized units following the expressions of Eq. (3).

For example, if one uses a $Bi_{12}TiO_{20}$ (BTO) crystal, by choosing $X_0 = 10$ μm, a HeNe laser beam of 10 mW/cm^2 and a artificial dark irradiance of 1 mW/cm^2, one obtains $r = 10$, a screening soliton HWHM of 20.64 μm, and $Z_0 = 2.52$ mm. In this particular case, the width of the image along x is 64 μm and the real length along z is 25.8 mm. Considering $r_{eff} = 5$ pm/V, one must apply an electric field of 9.764 kV/cm to achieve $N = 1$.

A. Convergence toward a screening soliton

In the first calculation, we study the behavior of a soliton beam with an input beam profile equal to $U(X,0,0) = \sqrt{r}\gamma(X,\infty)$. This means that we introduced, on the entrance face of the crystal, the steady-state screening soliton profile. The conditions of the calculation are $N = 1$, $D = 0$, and $r = 10$. The zero value of D is connected to neglecting the diffusion. The r value higher than 3 corresponds to a screening soliton with a diameter twice larger than the minimum of the existence curve (the so-called quasi-steady-state soliton) [11,13,17].

Figure 1 represents the four images at $\tau = 0$, 0.2, 0.5, and 1. Our calculations show that, for $r = 10$, the beam appears to overfocus somewhere along the Z direction and reproduces this scheme quasiperiodically along it (if a longer crystal had been considered in the calculation). This overfocusing has been hinted to be maximum at $\tau = 0.2$ (in fact $\tau = 2/r$), which corresponds to the quasi-steady-state soliton [11,17]. Thus the initial profile goes transiently through the quasi-steady-state, then progressively [Fig. 1(c)] relaxes towards a pure screening soliton solution exhibiting a HWHM equal to that of the entrance beam (HWHM=2.064). The calculation for $\tau = \infty$ gives a beam profile roughly constant along the Z axis. Figure 1(e) shows the comparison between the beam profiles on the entrance face of the crystal and at the point where it is narrowest in Fig. 1(b), which corresponds to the maximum of the overfocusing effect.

B. Evolution from the quasisteady state soliton to a less focalized state

In the second part of our calculations (Fig. 2), we chose the entrance profile to correspond to that of the quasi-steady-state soliton (i.e., minimum waist in time) $U(X,0,0) = \sqrt{r}\gamma(X,2/r)$ at the predicted time $\tau = 2/r$. We set the following parameters: $N = 1$, $D = 0$, and $r = 100$. The calculations reported were done at $\tau = 0$, $\tau = 0.02 = 2/r$, $\tau = 0.25$, and $\tau = 1$.

Our simulations clearly show that the initial natural diffraction at $\tau = 0$ focuses at $\tau = 0.02$ [Fig. 2(b)], a time corresponding to the build up of the quasi-steady-state soliton. The beam profile at that time is the same as on the crystal entrance. Then, since we are in a transient regime, (which means that this soliton has a limited lifetime), the beam eventually diffracts progressively towards a less focused state.

C. Occurrence of a non-quasi-steady-state transient soliton

The introduction on the entrance face of the crystal of a light profile satisfying Eq. (7), but corresponding to a time
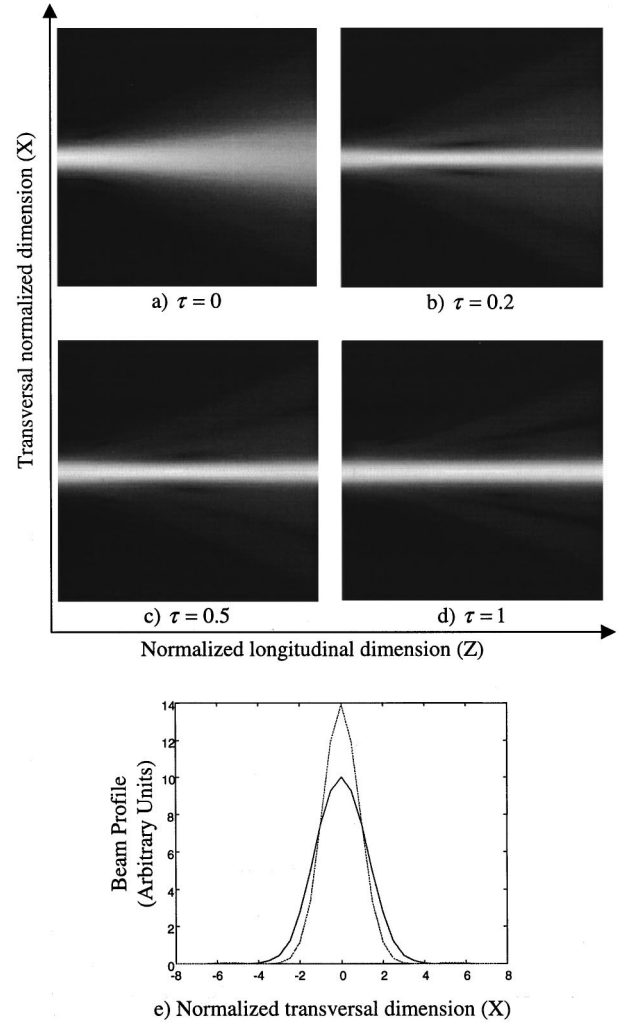

FIG. 1. Convergence to the screening soliton. The calculation parameters are $N = 1$, $D = 0$, $r = 10$ with the input profile $U(X,00) = \sqrt{r}\gamma(X,\infty)$. (a) $\tau = 0$, (b) $\tau = 0.2$, (c) $\tau = 0.5$, (d) $\tau = 1$ which is similar to $\tau = \infty$. (e) reports a comparison between the screening soliton profile and the beam profile at the minimum width in (b). X goes from -32 to $+32$, Z from 0 to 10.24. In accordance with the example given in Sec. III, it is important to note the difference between scaling factors X_0 and Z_0.

$(1/r)$ shorter than of the quasi-steady-state $(2/r)$ demonstrates that obtaining a transient soliton behavior at $\tau = 1/r$ is possible. This is clearly seen on Fig. 3(b), for which an entrance profile $U(X,0,0) = \sqrt{r}\gamma(X,1/r)$ is introduced: we computed the propagation profiles at times $\tau = 0$, $\tau = 0.01 = 1/r$, $\tau = 0.05$, and $\tau = 1$.

Our calculations evidence that, at the time at which the transient soliton is expected, the HWHM is unchanged throughout the propagation. It corresponds to the beam profile on the entrance face of the crystal [Fig. 3(b)]. This confirms the soliton character of this particular solution at $\tau = 0.01$.

D. Influence of the beam shape on the soliton propagation

The transient soliton solutions exhibit a particular property: another soliton solution having the same HWHM can exist, but at another time. For instance the soliton solution at
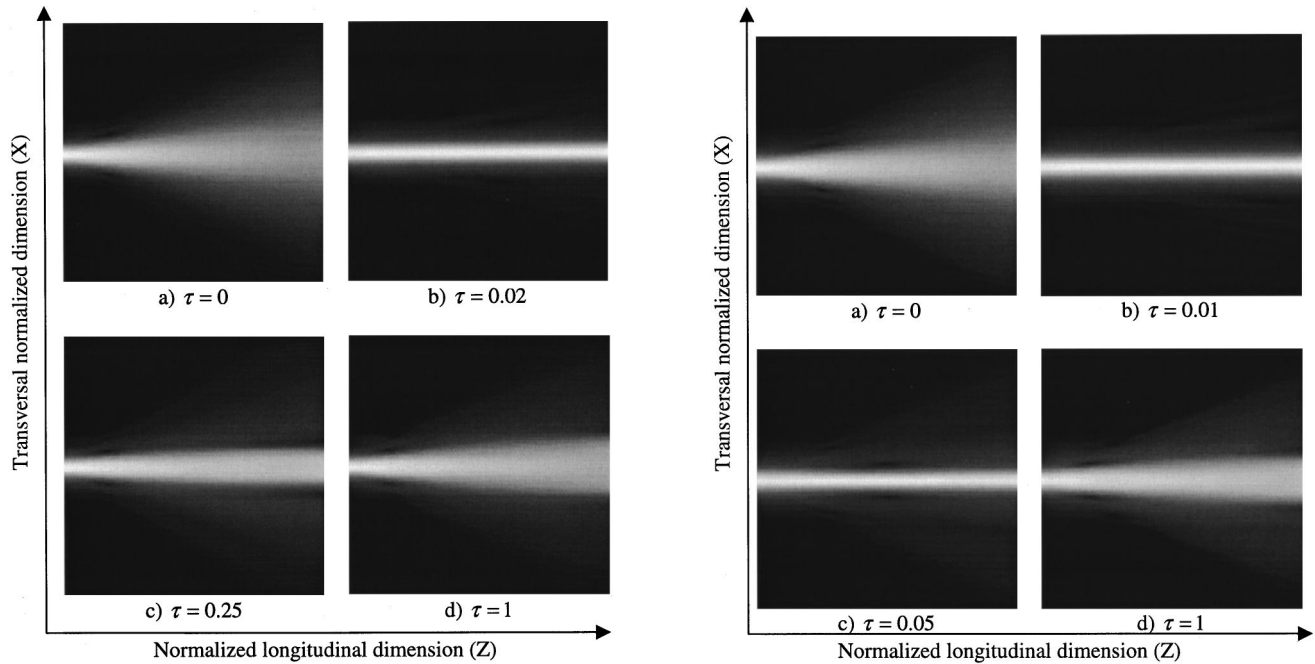
FIG. 2. Occurrence of a transient quasi-steady-state soliton. The calculation parameters are $N=1$, $D=0$, $r=100$ with an input profile equal to $U(X,00)=\sqrt{r}\tau(X2/r)$. (a) $\tau=0$, (b) $\tau=0.02=2/r$, (c) $\tau=0.25$, (d) $\tau=1$. X goes from -32 to $+32$, Z from 0 to 10.24.

$\tau=0.01$ has the same HWHM as the solution for $\tau=0.05$. This case is reported in Fig. 3, the two profiles of the considered solitons being shown in Fig. 3(e). Our illustrations show the beam computed at time $\tau=0.05$ [Fig. 3(c)] with an entrance beam profile corresponding to the transient solution at $\tau=0.01$. The overfocusing observed evidences that the time $\tau=0.05$ does not correspond to a soliton propagation. However, the introduction of the beam profile corresponding to the soliton solution at $\tau=0.05$ would have allowed a soliton propagation at that particular time. These features are explained by the differences in the profiles of the entrance beams since their HWHM are the same. They consequently point out the role of the profile shape.

E. Numerical simulation of drift combined with diffusion transport mechanisms

As previously mentioned, the $(1+1)$D theory of solitons in photorefractive media generally neglects the diffusion term in the band-transport model, which is known to be responsible for self-bending effects [5,14]. In this part of the simulation, the diffusion term has been kept in the wave equation (2) and is included in the parameter D.

Figure 4 reports the propagation of a laser beam with initial conditions equivalent to the screening solitons and with the calculation parameters $N=1$ and $r=10$ (as in Fig. 1), but with $D=0.1$. Our calculations, performed at $\tau=0$, $\tau=0.2$, $\tau=0.25$, and $\tau=1$, indicate the installation of a progressive bending of the light beam in direction of the c axis (given by the sign of D).

A careful observation of the successive Figs. 4(a)–4(f) evidences a rather significant self-focusing effect preceding a progressive installation of the bending process in the direction of the c axis. The numerically calculated phenomenon is
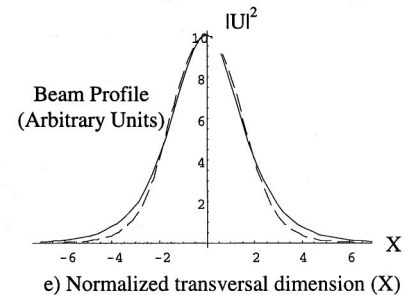

FIG. 3. Evolution through a transient non-quasi-steady-state soliton. The calculation parameters are $N=1$, $D=0$, $r=100$ with initial conditions $U(X,00)=\sqrt{r}\gamma(X,1/r)$. (a) $\tau=0$, (b) $\tau=0.01=1/r$, (c) $\tau=0.05=\tau_1$, (d) $\tau=1$, (e) comparison between soliton profiles at $\tau=0.01$ (solid line) and at $\tau=0.05$ (dotted line), $\tau=1$. X goes from -32 to $+32$, Z from 0 to 10.24.

in accordance with the previous results given by Christodoulides *et al.* [14] and Krolikowski *et al.* [18]. Furthermore, our calculations also show an asymmetry in the beam profile, with higher intensities on the inside beam curvature. This feature may have some analogy with the self-steepening effect [15]. Experimental hints of such behaviors have been reported on $BaTiO_3$ [17].

F. Simulation of optical branching

Several authors discussed the stability conditions of photorefractive spatial solitons and the robustness of the self-trapped propagation against localized perturbations [19–23]. Contrary to what happens in Kerr-like media, photorefractive screening solitons are shown to be stable as long as the material and the propagation parameters are along the existence curve [14]. On the other hand, Jerominek *et al.* [16] observed propagation of a light beam in photorefractive $LiNbO_3$ accompanied with what he called optical branching, namely, the division of the optical beam in several branches. It is, however, important to point out that the experimental conditions used by Jerominek correspond to the presence of high negative nonlinearities, responsible for dark solitons.
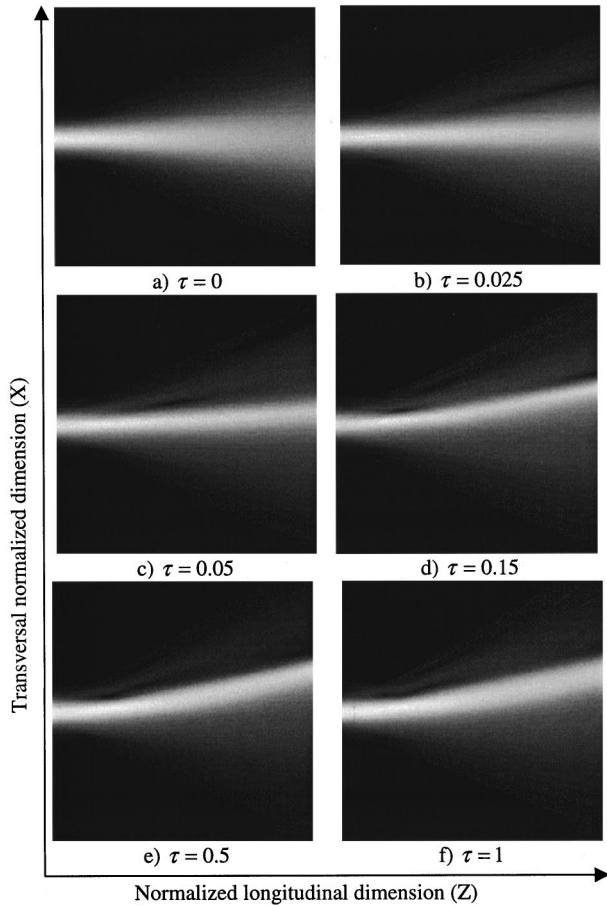
FIG. 4. Evidence of beam bending. The calculation parameters are $N=1$, $D=0.1$, $r=10$, with an input profile $U(X,00) = \sqrt{r}\gamma(X,\infty)$. (a) $\tau=0$, (b) $\tau=0.025$, (c) $\tau=0.05$, (d) $\tau=0.15$, (e) $\tau=0.5$, and (f) $\tau=1$. X goes from -32 to $+32$, Z from 0 to 10.24.

Figure 5 shows a simulation of that phenomenon by taking the initial profile of the screening soliton calculated from Eqs. (7) and (8) with $N=1$ and $r=10$, and using $N=5$ (i.e., high nonlinearity) and $D=0.1$ for the computation of the propagation. It can be observed that the beam strongly self-focuses at a distance shorter than the diffraction length. It then divides in several branches (or filaments), propagating as bending solitons. The bending effect is due to the nonzero value of D. It is remarkable that the diameter of the branches is significantly narrower than the initial screening soliton. On the other hand, the closely neighboring branches develop interactions between each other [9,10,22]. Additionally, we can note that the characteristics of the branches seem to respect the existence curve of the solitons. For instance, the upper branch in the steady state configuration on Fig. 5(d) can be defined by its ratio to dark irradiance $r=1.87$ and its HWHM of 0.9.

The simulation presented in Fig. 6 corresponds to calculations equivalent to that of Fig. 5, but with parameters N and D close to those expected for the BaTiO$_3$ crystal, taking into account the physical parameters of this crystal. The external field applied is equal to 10 kV/cm, the entrance beam waist is 15 μm and the propagation length is about 7 mm. Our calculations evidence quasiperiodic self-focusing, as well as diffracting branches of smaller intensity bending in the two transverse directions. Experiments on photorefractive
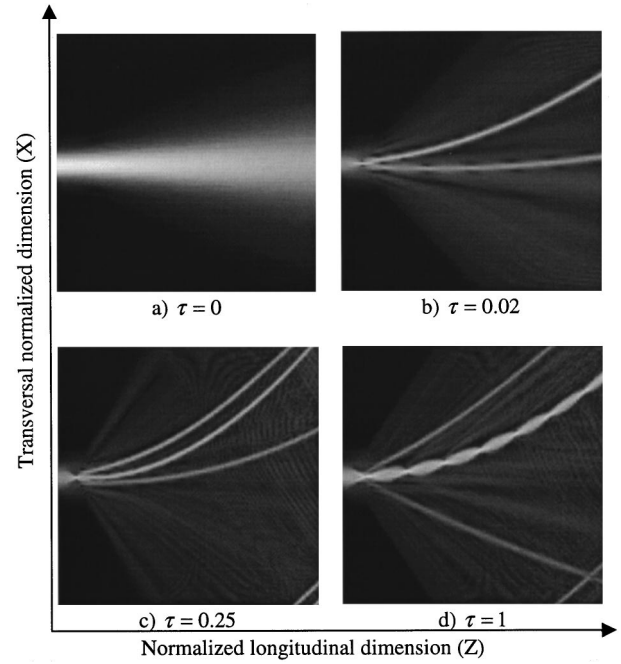

FIG. 5. Optical branching in photorefractive media. The calculation parameters are $N=5$, $D=0.1$, $r=10$, with an input profile $U(X,00)=\sqrt{r}\gamma(X,\infty)$. (a) $\tau=0$, (b) $\tau=0.02$, (c) $\tau=0.25$, (d) $\tau=1$. X goes from -32 to $+32$, Z from 0 to 10.24.

BaTiO$_3$ crystals are on the way and seem to confirm some elements of our calculations [17].

It is important to note that N depends on an arbitrary space scale factor x_0. Therefore, an increase in the value of
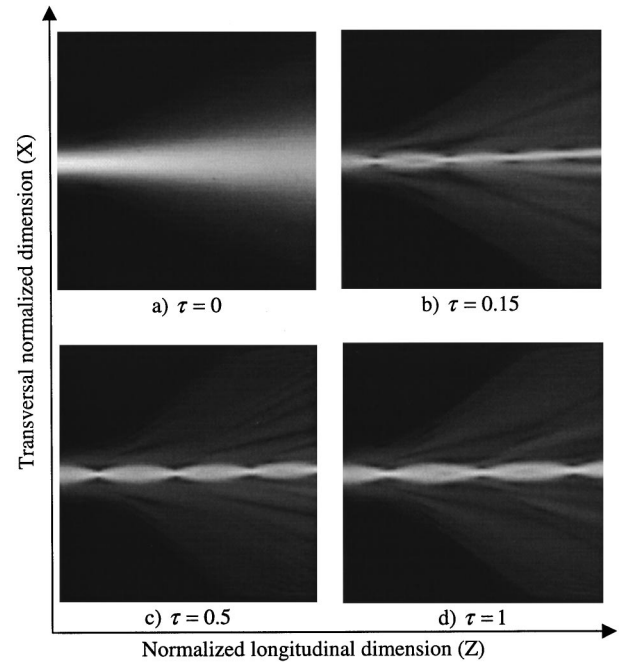

FIG. 6. Optical branching in photorefractive BaTiO$_3$. The calculation parameters, taken in accordance with the corresponding physical values of BaTiO$_3$ are $N=2.25$, $D=0.01$, $r=10$. The applied electric field is 10 kV/cm. The input profile is $U(X,00) = \sqrt{r}\gamma(X,\infty)$, the waist being equal to 15 μm. (a) $\tau=0$, (b) $\tau=0.15$, (c) $\tau=0.5$, (d) $\tau=1$. X goes from -32 to $+32$, Z from 0 to 10.24.

N can be either seen as an increase of the electric field (or any other parameter in N) or as a decrease of the scale factor: both interpretations lead to the fact that if N is increased whereas the input profile is not changed, the one screening soliton that can exist is significantly narrower than the input profile. Our calculations show that the self-focusing phenomenon is unstable if the input profile is far wider than the soliton diameter. Our calculations are confirmed by a similar bidimensional steady-state prediction by Mamaev *et al.* [23]

IV. CONCLUSION

In this paper, we evidenced the temporal behavior of photorefractive self-focusing and spatial solitons through BPM numerical simulations performed on the basis of a $(1+1)D$ model of laser light propagation in photorefractive media. Our numerical simulations show the following essential features.

Our numerical data confirm, by comparison with the experimental data [17], the validity of the space charge field and nonlinear wave equation used. Indeed, the fact to take initial conditions with quasi-steady-state and screening solitons effectively shows transient occurrence of the quasi-steady-state and stable convergence to the screening soliton. This presents an *a posteriori* validation of the assumption made in our previous publications [11,13].

The simulation establishes a strong stability of the model, as long as the calculation parameters are close to the soliton existence curve. Indeed, it confirms that the $(1+1)D$ model is stable. Furthermore, since our calculations satisfactorily describe the experimental data, which of course correspond to a $(2+1)D$ system, this indicates that the $(2+1)D$ system is also stable and that a $(1+1)D$ system is able to simulate a real system with good accuracy.

The model used here allows us, not only to simulate soliton propagation, but also to study more sophisticated phenomena such as optical branching.

[1] M. Segev, B. Crosignani, and A. Yariv, Phys. Rev. Lett. **68**, 923 (1992).

[2] B. Crosignani, M. Segev, D. Engin, P. Di Porto, A. Yariv, and G. Salamo, J. Opt. Soc. Am. B **10**, 446 (1993).

[3] G. C. Duree, J. L. Schultz, G. J. Salamo, M. Segev, A. Yariv, B. Crosignani, P. Di Porto, E. J. Sharp, and R. R. Neurga-onkar, Phys. Rev. Lett. **71**, 533 (1993).

[4] M. D. Iturbe Castillo, P. A. Marquez Aguilar, J. J. Sanchez Mandragon, S. Stepanov, and V. Vysloukh, Appl. Phys. Lett. **64**, 408 (1994).

[5] D. N. Christodoulides and M. I. Carvalho, Opt. Lett. **19**, 1714 (1994).

[6] G. C. Valley, M. Segev, B. Crosignani, A. Yariv, M. M. Fejer, and M. C. Bashaw, Phys. Rev. A **50**, R4457 (1994).

[7] M. Segev, M. Shih, and G. J. Valley, J. Opt. Soc. Am. B **13**, 706 (1996).

[8] M. Morin, G. Duree, G. Salamo, and M. Segev, Opt. Lett. **20**, 2066 (1995).

[9] M. Shih and M. Segev, Opt. Lett. **21**, 1538 (1996).

[10] M. Shih, M. Segev, and M. Salamo, Phys. Rev. Lett. **78**, 2551 (1997).

[11] N. Fressengeas, J. Maufoy, and G. Kugel, Phys. Rev. E **54**, 6866 (1996).

[12] N. V. Kukhtarev, V. B. Markov, S. G. Odulov, M. S. Soskin, and V. L. Vinetskii, Ferroelectrics **22**, 949 (1979).

[13] N. Fressengeas, J. Maufoy, D. Wolfersberger, and G. Kugel, Opt. Commun. **145**, 393 (1998).

[14] D. N. Christodoulides and M. I. Carvalho, J. Opt. Soc. Am. B **12**, 1628 (1995).

[15] G. P. Agrawal, *Nonlinear Fiber Optics* (Academic, London, 1989).

[16] H. Jerominek, C. Delisle, and R. Tremblay, Appl. Opt. **25**, 732 (1986).

[17] N. Fressengeas, Thèse de l'Université, Université de Metz, 1997 (unpublished).

[18] W. Kròlikovski, N. Akhmediev, D. R. Andersen, and B. Luther-Davies, Opt. Commun. **132**, 179 (1996).

[19] K. Kos, H. Meng, G. Salamo, M. Shih, M. Segev, and G. Valley, Phys. Rev. E **53**, R4330 (1996).

[20] M. Segev, B. Crosignani, P. Di Porto, G. C. Duree, G. Salamo, and E. Sharp, Opt. Lett. **19**, 1296 (1994).

[21] A. V. Mamaev, M. Saffman, and A. A. Zozulya, Europhys. Lett. **35**, 25 (1996).

[22] W. Krolikowski and S. A. Holmstrom, Opt. Lett. **22**, 369 (1997).

[23] A. V. Mamaev, M. Saffman, D. Z. Anderson, and A. A. Zozulya, Phys. Rev. A **54**, 870 (1996).